MATERIALS CHEMISTRY FRONTIERS

CCS 中国化学会 CHINESE CHEMICAL SOCIETY

ICCAS

ROYAL SOCIETY OF CHEMISTRY

Effects of Additive NH3 with Citric Acid in Precursor and Controlling Deposited Thickness for Growing MoO3 Crystals and Nanorods

Journal:	*Materials Chemistry Frontiers*
Manuscript ID	QM-RES-07-2020-000535.R3
Article Type:	Research Article
Date Submitted by the Author:	04-Oct-2020
Complete List of Authors:	Hirose, Yukiko; Osaka University Institute of Science and Industrial Research Sugahara, Tohru; Osaka University, The Institute of Scientific and Industrial Research (ISIR), Nakamura, Jun-ichi; Nippon Shiokubai Co., Led. Harada, Nobuyuki; Nippon Shokubai Research Alliance Laboratories Suganuma, Katsuaki; Osaka University,

Effects of Additive NH_3 with Citric Acid in Precursor and Controlling Deposited Thickness for Growing Molybdenum Oxide Crystals and Nanorods

Yukiko Hirose[1], Tohru Sugahara[1*], Jun-ichi Nakamura[2,3*], Nobuyuki Harada[2], and Katsuaki Suganuma[1]

1. Department of Advanced Interconnection Materials, The Institute of Science and Industrial Research, Osaka University, 8-1 Mihogaoka, Ibaraki, Osaka, 567-0047, Japan.
2. Nippon Shokubai Research Alliance Laboratories, 2-1 Yamadaoka, Suita, Osaka, 565-0871, Japan.
3. Nippon Shiokubai Co., Led., 5-8 Nishi Otabi-cho, Suita, Osaka, 564-0034, Japan.

Corresponding Authors: Tohru Sugahara (sugahara@sanken.osaka-u.ac.jp), Jun-ichi Nakamura (jun-ichi_nakamura@shokubai.co.jp)

ABSTRACT

In recent years, authors have successfully established a simple method for the production of fine single crystal-like α-MoO_3 nanorod structures on substrates using a solution metal-organic decomposition (MOD) method to deposit film coatings. However, to grow α-MoO_3 nanorods by the MOD method, an accurate mechanism between α-MoO_3 nanorod extension and precursor preparation (contents of precursor conditions) should be identified. Here, we demonstrated controllable α-MoO_3 nanorods and plat-like α-MoO_3 crystal growth based on as-deposited film thickness by using different citric acid (CA) and ammonia (NH_3) ratios in the precursor solutions. The α-MoO_3 nanorods growth mechanisms are discussed in detail with the precursor conditions and deposition film thickness; excellent results were achieved in controlling the film thickness by preparation of the precursors viscosities. In addition, the CA and NH_3 amount effects of the α-MoO_3 nanorods and crystal growth were investigated. It was found that the NH_3 plays an effective role in delaying the decomposition timing of CA, promotes the growth of α-MoO_3 nanorods, and reduces the growth and increase of plate-like α-MoO_3 crystals. The study obtained excellent results for the growth extension of α-MoO_3 nanorods and plate-like α-MoO_3 crystals, controlled by film thickness as the role of CA and NH_3. The demonstrated strictly controlled α-MoO_3 nanostructure forming process can be achieved with the solution MOD method.

INTRODUCTION

In recent years, molybdenum (Mo) compounds have attracted considerable attention for their properties, such as the various valences of Mo, the presence of many crystal structures, and the complex band structure. In particular, many reports in the past decade were published due to broad applications, such as catalyst[1,2], electrode[3,4], semiconductor[5,6], sensor[7,8,9], organic devices[10,11,12], electrochromic[13,14], and photochromic[15]. For example, Mo oxides are very useful as an electronic catalyst owing to their high electron affinity. Since the Mo cation makes octahedral or tetrahedral coordination with anions such as oxygen, sulfa, and other chalcogens in compounds that are easy to distort and react with the other cation of various elements. The Mo complex compounds, therefore, have been widely investigated as cooperative catalysts[1], and α-MoO_3 can be used as hybrid catalysts, which have been broadly investigated as cooperative catalysts with various elements. Moreover, Mo is well known for its various valences from divalent to hexavalent, and compounds containing quadrivalent, pentavalent, and hexavalent in the oxygen states. Various types of Mo oxides are found in stoichiometric and non-stoichiometric oxides, such as MoO_2 (Ⅳ), Mo_2O_5 (Ⅴ), and MoO_3 (Ⅵ). Non-stoichiometric Mo oxides have oxygen vacancies, with average values of various types of sub-oxides between 6.0 and 4.0. Mo oxides have variety of electron band structures are expected to use from metals to wide-gap semiconductors.

Nanostructure materials and two-dimensional materials of compounds, and oxides, are widely applied to next-generation functional clean energy applications[16] such as electric devices and catalyst for chemical reaction[17] due to the characteristic electronic structures and physical properties of the materials. In particular, nanostructured materials and two-dimensional materials of Mo compounds typified by α-$MoO_{3-\delta}$ have an excellent property[18]. More precisely, it is electrode reaction speed up by the high ratio surface area and the abilities of quick electric accumulation and discharge. It is expected to be a new material for supercapacitors or lithium ion batteries (LIBs)[19,20]. Nanostructured Mo compounds have a large specific surface area and unique chemical and physical properties. Notably, the characteristic properties are crucial for these multiple electronic devices.

In addition, forming and controlling nanostructures is an essential issue; nanostructured Mo compounds have been fabricated by a wide variety of methods, such as hydrothermal synthesis,[21] PVD,[22] RF magnetron sputtering[23,24], thermal evaporation, and molecular beam epitaxy. However, these methods consume significant amounts of energy and material recources, implying that they are un-eco-friendly. In recent years, the authors have focused on synthesis as fine as nanostructured oxide materials by the metal-organic decomposition (MOD)[7, 12,25,26,27,28,29]. The MOD method is consuming low energy, and is environment friendly, it can contribute to the realization of the sustainable society.

We found that the α-MoO_3 nanorods initially grew from spin-coated thin films after sintering at 673 K for several minutes. Subsequently, the α-MoO_3 nanorods underwent a transition to the plate-like α-MoO_3 phase while continuously sintering for a long time (over approximately 20 min, as illustrated in Fig. SI-1), which was discussed with physical properties by the gas sensing, and chemical compassion by XRD and TEM in a previous paper[7,25]. However, the behavior of the seed layer thickness with sintering time and the transitions were uninvestigated in detail. When the experimental conditions, for example, molar ratio, mixing starting materials, and spin coating, are changed for several reasons, the growth of α-MoO_3 nanorod arrays and the transition timing are significantly different depending on the experimental restriction, as illustrated in Fig. SI-1 and SI-2. The molybdenum oxide thin films obtained after sintering at 673 K for 15 min (in Fig. SI-1) from the same precursor and the same coating conditions were significantly different film structures from the other precursor and coating conditions after sintering for 15min (Fig. SI-2).

The α-MoO_3 nanorods growth mechanism and relationship of the transition timing is assumed to depend on each experimental condition, the authors had been discussed with TG/DT analysis and concluded a critical role of decomposition timing of CA in the precursor, but unclarified in the previous studies[7,25] Although the CA contributes to the growth of α-MoO_3 nanorods, it has been uncontrolled precisely due to the lack of clarity in the details of the α-MoO_3 nanorod growth mechanism. In addition, the thicknesses of the seed layers, which are

the under layers of the α-MoO_3 nanorods, have been insufficiently investigated with α-MoO_3 nanorods growth.

In this study, the growth and elongation of α-MoO_3 nanorods were investigated with the content effects of CA and NH_3 on Mo in the precursor. The relationship between the α-MoO_3 nanorods/plate-like α-MoO_3 crystal growth and the as-deposited coating thickness are discussed with the seed layer thicknesses. In addition, here we demonstrated the formation of a transparent α-MoO_3 nanorods thin-film sample in which the α-MoO_3 nanorods can be extended up to one micrometer, and the seed layer thickness can be reduced by approximately 50 nm by using the processing method of this study. The molybdenum oxide thin-film structures, such as the α-MoO_3 nanorods length, the seed layer thickness, and the plate-like α-MoO_3 crystals numbers, were precisely controlled by several experimental parameters, such as the amount of CA and NH_3 and the spin-coating thickness of the precursor.

EXPERIMENTAL

Ammonium molybdate ($H_8N_2O_4Mo$), ammonium molybdate tetrahydrate ($(NH_4)_6Mo_7O_{24}$ $4H_2O$), tri-ammonium citrate ($(NH_4)_3C_6H_5O_7$)), CA ($C_6H_8O_7$), and N, N-dimethylformamide(DMF) (C_3H_7NO (10 mL)) purchased from Fujifilm Wako Pure chemical, Japan were used in this experiment. Each pair of ammonium molybdate and CA, ammonium molybdate tetrahydrate and CA, tri-ammonium citrate adjusted ammonium molybdate tetrahydrate and CA, were dissolved in 10 mL of DMF at respective ratios to obtain solution precursors with Mo concentrations ranging from 0.4 to 1.0 M. These precursors were stirred and dissolved with magnetic stirring at room temperature for 1 day to 14 days until clear and homogeneous solutions were obtained.

For the synthesis of Mo oxide nanocrystals, the precursor was spin-coated at 1000–5000 rpm (MIKASA SPINCOATER 1H-DX2, Tokyo, Japan) on a silica glass substrate after cleaning with N_2 plasma for 90 s. The deposited thin film was sintered at 673 K for 15 min in an electric furnace (DENKEN KDF-P90, Kyoto, Japan) or a temperature of 373 K for 15 min (AS ONE Electric Oven NEXAS series, OFX-50, Tokyo, Japan) to obtain thin film samples.

The top and cross-section morphological studies were carried out using field-emission scanning electron microscopy (FE-SEM) (Hitachi SU8020, Tokyo, Japan). The values of viscosity were measured by Viscometer (TOKI SANGYIO VISCOMETER TV-25 Type L) at

298 K. The thickness after sintering at 373 K for 15 min was verified using a laser microscope (KEYENCE VK-9510).

RESULTS AND DISCUSSION

Fine almost single crystal α-MoO_3 nanorods grow from substrate which investigated by XRD and TEM studies in the previous study[25]. The longest α-MoO_3 nanorods were obtained as the molar at the ratio of molybdenum (Mo), CA, and ammonium (NH_3) = 1:3:2 (0.5:1.5:1.0) in the previous study.[7,25] Because the effect between the ratios of CA in the precursors and the coating process properties will be discussed in detail, three kinds of precursors with ratios of 1:3:2, 1:4:2, and 1:6:2 in 0.5 M were prepared in this experiment. Table 1 summarizes the precursor viscosities and the other experimental conditions of each precursors. The precursor viscosities increased with increasing concentrations of CA in the precursors, as shown in Table 1. The viscosity of 1:4:2 is approximately 20 mPa·s, two times as large as the 1:3:2 precursor, and the viscosity of 1:6:2 was 90 mPa·s, which is nine times higher than that of the 1:3:2 precursor.

To fix the thickness of the as-deposited precursor, spin coating was performed in a preliminary experiment with three types of precursors. The fixed spin-coating conditions were

1500, 2000, and 3000 rpm of each the 1:3:2, 1:4:2, and 1:6:2 precursors, respectively, which were determined to be approximately 1 μm of the film thickness after sintering at 473 K.

Figure 1a-1 – c-3 show the FE-SEM images of the molybdenum oxide thin-film samples obtained by growing on silica glass substrate after sintering at 673 K for 15 min, under the same conditions as in the preliminary experiment, that is, 1500 rpm of 1:3:2 precursor, 2000 rpm of 1:4:2 precursor, and 3000 rpm of 1:6:2 precursor, respectively. The top-view low magnification (×50,000) and high magnification (×100,000) FE-SEM images of the film samples are shown in Fig. 1a-1 – c-1 and 1a-2 – c-2, respectively. The cross-sectional FE-SEM images of the film samples are displayed in Fig. 1a-3 – c-3. As Fig. 1a-1 – c-3 illustrate, the MoO_3 nanorods grew on the SiO_2 glass substrate. The α-MoO_3 nanorods grew almost uniformly on the surface of these samples, and the α-MoO_3 nanorods length and the density on the film samples increased with increasing CA ratio in the precursors. The diameters of the α-MoO_3 nanorods were almost the same at approximately 10 nm with changes in the other CA concentrations, as shown in the FE-SEM images in Fig. 1 a-2 – c-2. In addition, the α-MoO_3 nanorods curved structure, and the curvatures are strong due to an increase in the CA ratio, as illustrated in Fig. 1 a-2, b-2, and c-2.

Fig. 2a shows the eye catch schematic figure of the cross-sectional image of the molybdenum oxide thin-film samples. In the cross-sectional FE-SEM images of Fig. 1 a-3 – c-

3, molybdenum oxide thin-film layers exist between the SiO_2 substrate and the α-MoO_3 nanorod structures, as shown in Fig. 2a. The layers are called seed layers because the α-MoO_3 nanorods are grown from the seed layers, to decrease the thickness gradually with extending the sintering time, as shown in the FE-SEM images in Fig. SI-1 and SI-2. The thickness of the seed layers decreased with increasing CA ratio, and the total thickness of the seed layers and the α-MoO_3 nanorod structure layers of these three samples look equivalent, as shown in Fig. 1a-3 – c-3. It implies that the growth mechanism is strongly related to the as-deposited thickness (or volumes) of the precursors and the concentration of CA in the precursors.

From the top-view FE-SEM and cross-sectional FE-SEM images of Fig. 1, the lengths of the longest α-MoO_3 nanorods and the thickness of the seed layer were measured and plotted in the graph of Fig. 2b. The data imply that the length of the α-MoO_3 nanorods increased with increasing CA ratio. The longest length of the α-MoO_3 nanorods was 400 nm at 1:3:2, 500 nm for 1:4:2, and 1000 nm for 1:6:2. In contrast, the thicknesses of the seed layers decreased from approximately 200 nm of 1:3:2, 100 nm of 1:4:2, and up to 50 nm of 1:6:2, respectively, as the ratio of CA increased. Although the film thicknesses of these three samples were almost identical before sintering, the quantity of Mo included per unit volume is estimated to decrease with increasing CA ratio. This indicates that the length of the α-MoO_3 nanorods increases with increasing CA ratio, despite the decrease in the amount of Mo per unit volume. It implies that the inclusion ratio of CA in the precursors has a significant influence on the growth and

extension of α-MoO_3 nanorods.

Owing to the almost fixed as-deposited thin-film thicknesses before sintering by spin coating, the α-MoO_3 nanorods growth can be discussed with the seed layer thickness and CA amount in the precursors. When an extremely large amount of CA is included in the precursor, the seed layer may become thin, and the α-MoO_3 nanorods are easily grown. On the other hand, the seed layers may become thick and the α-MoO_3 nanorods are hardly grown when an extremely small amount of CA is present in the precursors. The α-MoO_3 nanorods may grow from the seed layer, as described above, in part of Fig. SI-1 and SI-2 because the seed layer thickness is related to the amount of CA in the precursor. The amount of CA played significant role in the α-MoO_3 nanorod growth, and the thicknesses of the seed layer decreased with α-MoO_3 nanorods growth due to the use of CA and Mo compounds in the as-deposited precursor films.

To investigate the effect of film thickness, four types of samples were prepared with different spin-coating conditions using precursors with a fixed molar ratio of Mo, CA, and NH_3 (0.4. mol/L and 1:6:2). Fig. 3a-1 – d-3 show FE-SEM images after sintering at 673 K for 15 min of four kinds of molybdenum oxide thin-film samples obtained on silica glass substrates with spin-coating conditions of 1500, 2000, 2500, and 5000 rpm. The top-view low magnification (×10,000) and high magnification (×50,000) FE-SEM images of the film

samples are shown in Fig. 3a-1 – d-1 and 3a-2 – d-2, respectively. The cross-sectional FE-SEM images of the film samples are displayed in Fig. 3a-3 – d-3. The decrease in the number of α-MoO_3 nanorods and the increase in the number of, plate-like α-MoO_3 crystals which are reported in the previous study, [7, 25] were observed with increasing spin-coating speeds, as shown in Fig. 3a-1 – d-2. Approximately 500 nm in length and the growth density of the α-MoO_3 nanorods are almost the same as those shown in Fig. 3a-2 – c-2. The size of the plate-like α-MoO_3 crystals was observed from submicron to a few microns (Fig. 3d-1 and d-2). The thickness of the seed layers decreased with increasing spin-coating speeds, as shown in Fig. 3a-3 – d-3. In particular, the seed layer thickness of the 5000 rpm sample is very thin (approximately 5 nm), with a few α-MoO_3 nanorods and almost observing the plate-like α-MoO_3 crystals (Fig. 3d-1 and d-2). Even though the thicknesses of the seed layer decreased from 200 nm to 60 nm, the length and diameter of the α-MoO_3 nanorods were almost identical, as shown in Fig. 3 a-3, b-3, and c-3. Fig. 2c and 2d show that the color of the samples depends on the thickness of the seed layer.

Using the methods employed in this study, the seed layer can be controlled without changing the growth length of α-MoO_3 nanorods. The authors demonstrated that two kinds of seed layer thickness can be successfully coated with the spin-coating conditions of 1500 rpm and 2500 rpm. The α-MoO_3 nanorods length are approximately 400 nm, as displayed in Fig. 2c and 2d, have seed layer thicknesses of approximately 200 nm and approximately 50 nm,

respectively. The approximately 200 nm thick seed layer sample showed a transparent dark brown color, but the approximately 50 nm thick seed layer sample was transparent light brown. The results from these images imply that the seed layer thickness strongly correlated with the transparency, related without α-MoO_3 nanorods length and density.

Figure 4 shows the number of α-MoO_3 nanorods and plate-like α-MoO_3 crystals, which were measured from the FE-SEM images in Fig. 3. The number of α-MoO_3 nanorods per arbitrary unit area decreased sharply around at approximately 40 nm of the seed layer thickness. In contrast, the number of plate-like α-MoO_3 crystals per arbitrary unit area increased sharply at almost identical seed layer thickness. These data imply that each of the numbers of α-MoO_3 nanorods and plate-like α-MoO_3 crystals are opposite of increasing or decreasing behavior at the critical seed layer thickness, as shown in Fig. 4. This indicates that we can control the number of α-MoO_3 nanorods and/or plate-like α-MoO_3 crystals by controlling the seed layer thickness.

To investigate the effect of including the molar ratios of Mo, CA, and NH_3 in the precursors, seven kinds of precursors were prepared in this experiment. The molar concentrations of precursors were 0.5 M and 1.0 M, and the including molar ratio of Mo, CA, and NH_3 were A(1:6:2), B(1:4:2), C(1:3:2), D(1:3:2), E(1:3:1), F(1:3:1), and G(1:1:1), respectively. Table 2 summarizes the mixing conditions of all precursor solutions used in this

experiment, and the Mo contents show wt% in the solute and the other experimental conditions of each precursor. By fixing Mo to NH_3 ratios into 1:2, three kinds precursors of A(1:6:2), B(1:4:2), and C(1:3:2) were prepared, while the other three kinds precursors, E(1:3:1), F(1:3:1), and G(1:1:1), were prepared by fixing Mo:NH_3 into 1:1. The precursor D(1:3:2), with the same ratio as C(1:3:2), was prepared by the effect of the NH_3 amounts in the precursor using ammonium molybdate tetrahydrate. Because the same ratio of Mo:NH_3 (= 1:2) was adjusted to the precursor C(1:3:2), triammonium citrate was added with ammonium molybdate tetrahydrate and CA.

To fix the as-deposited film thickness, the spin-coating conditions were determined by preliminary experiments with seven kinds of precursors. Subsequently, the spin-coating conditions were fixed at 3000 rpm of the A(1:6:2) precursor, 2000 rpm of B(1:4:2) precursor, 1500 rpm of C(1:3:2) precursor, 1500 rpm of D(1:3:2) precursor, 1150 rpm of E(1:3:1) precursor, 3000 rpm of F (1:3:1) precursor, and 1100 rpm of G(1:3:2) precursor, respectively, which were determined to be approximately 1 to 1.8 μm after sintering at 473 K, as also displayed in Table 2.

Figure 5a-1 – d-3 show FE-SEM images after sintering at 673 K for 15 min of four types of molybdenum oxide thin-film samples (C, E, F, and G), which were obtained on a silica glass substrate with each spin-coating condition in Table 2. The top-view low magnification

(×10,000) and high magnification (×50,000) FE-SEM images of the film samples are shown in Fig. 5a-1 – d-1 and 5a-2 – d-2, respectively. The cross-sectional FE-SEM images of the film samples are displayed in Fig. 5a-3 – d-3.

The number of plate-like α-MoO_3 crystals increased as the concentration of NH_3 decreased. This is apparent in the comparison of Fig. 5a-1 and 5b-1. Similarly, comparing Fig. 5c-1 and d-1 shows that the number of plate-like α-MoO_3 crystals increased with decreasing CA concentration. The comparison of Fig. 5a-2 and b-2 demonstrates that the lengths of the α-MoO_3 nanorods are almost the same for different concentrations of NH_3. Meanwhile, comparing Fig. 5c-2 with d-2 shows that the length of the α-MoO_3 nanorods decreased with a decreasing concentration of CA. It is noteworthy that the seed layers of almost all samples consisted of two layers, as shown in Fig. 5c-3 and d-3; however, the detailed mechanism was not determined in this study.

Figure SI-3 shows top-view FE-SEM images of molybdenum oxide film samples with different NH_3 concentrations of C(1:3:2), D(1:3:2), and E(1:3:1). These samples were obtained on silica glass substrate after sintering at 673 K for 15 min, with the spin-coating conditions listed in Table 2. The α-MoO_3 nanorods of sample E(1:3:1) were grown straight; on the other hand, the α-MoO_3 nanorods of samples D(1:3:2) and C(1:3:2) were grown curling, as shown in Fig. SI-3. The sample D(1:3:2) was prepared by adding NH_3 amounts from sample E(1:3:1)

to adjust the same ratio of sample C(1:3:2). It is presumed that the α-MoO_3 nanorods underwent bending as the NH_3 concentration increased; however, the NH_3 role has not been clarified in this study.

To better understand these experiments, the measured values of the α-MoO_3 nanorod length, α-MoO_3 nanorod number, seed layer thickness, and plate-like α-MoO_3 crystal numbers are summarized with the amount ratio of NH_3/Mo, CA/Mo, and NH_3/CA, as shown in Fig. 6a – 6d. It is noteworthy that the number of α-MoO_3 nanorods and plate-like α-MoO_3 crystals were collected from the FE-SEM images divided into the grid of arbitrary unit aria. Fig. 6a indicates the length of the α-MoO_3 nanorods (triangles) and the thickness of the seed layer (circles) versus in the ratio of CA to Mo. These data were measured by top-view FE-SEM and cross-sectional FE-SEM images from the total of seven samples in Table 2 (including Fig. 5). The length of the α-MoO_3 nanorods increased and the thickness of the seed layer decreased, as the ratio of CA to Mo increased; it can be shown in Fig. 6a. This result implies that α-MoO_3 nanorods may not grow without the CA. Although the sample of the blue open circle symbol was three on the ratio of CA to Mo, the thickness of the seed layer was approximately 350 nm to deviate from the original tendency, which implies that its thickness may be observed around 200 nm. This is probably because the film thickness after sintering at 373 K is approximately 1.8 μm, which is thicker than that of the other samples, as shown in Table 2.

Fig. 6b shows the length of the α-MoO_3 nanorods (triangles) and the number of plate-like α-MoO_3 crystals per arbitrary unit area (circles) versus the ratio of CA to Mo. These data were collected from the top-view FE-SEM and cross-sectional FE-SEM images from a total of seven samples. As the ratio of CA to Mo increased, the number of plate-like α-MoO_3 crystals per arbitrary unit area decreased, and the length of the α-MoO_3 nanorods increased, as shown in Fig. 6b. More precisely, it is assumed that sufficient amount of CA is necessary to grow the α-MoO_3 nanorods while suppressing the growth of plate-like α-MoO_3 crystals. The blue open circle symbol samples were 3 – 4 in the ratio of CA to Mo, and the plate-like α-MoO_3 crystal numbers were 0 – 2, which deviated from the prospective tendency. Approximately 4–6 plate-like α-MoO_3 crystals were observed in these samples that had the expected tendency. This result strongly implies the NH_3 content effect with the ratio of the CA to Mo, suggesting the method to determine all parameters related to the ratio of amount of NH_3 to that of CA.

To determine the effect of the amount of NH_3 on the growth of α-MoO_3 nanorods and plate-like α-MoO_3 crystals, the ratio of NH_3 to Mo and NH_3 to CA in the precursors is discussed in this paragraph. Fig. 6c shows the number of α-MoO_3 nanorods (triangles) and the number of plate-like α-MoO_3 crystals per arbitrary unit area (circles) versus the ratio of NH_3/Mo. These data were collected from the FE-SEM images of all samples given in Table 2. As the ratio of NH_3 to Mo increased, both α-MoO_3 nanorods numbers and plate-like α-MoO_3 crystals numbers decreased, as shown in Fig. 6c. However, the number of plate-like α-MoO_3 crystals is affected

by the concentration of CA, as shown in Fig. 6b. To clarify the influence of the amount of NH_3 separating from the effect of CA amounts, the number of α-MoO_3 nanorods and plate-like α-MoO_3 crystals was segregated and plotted as a function of the ratio NH_3 to CA with a fixed ratio of CA to Mo in the inset graph of Fig. 6c. The inset graph of Fig. 6c demonstrates that the number of both α-MoO_3 nanorods and plate-like α-MoO_3 crystals decreased with an increase in the NH_3 to CA ratio. These results suggest that not only the amount of CA but also the amount of NH_3 have an effective role in the growth of both α-MoO_3 nanorods and plate-like α-MoO_3 crystals.

Fig. 6d shows plots of the length of α-MoO_3 nanorods (triangles) as a function of the NH_3 to Mo ratio. The lengths of the α-MoO_3 nanorods seem to extend with an increase in the NH_3 to Mo ratio, as shown in Fig. 6d. However, the length of the α-MoO_3 nanorods increased with an increase in the amount of CA. To determine the influence of the amount of NH_3, samples with the same ratio of CA to Mo are plotted with symbols of open triangles in Fig. 6d. These open triangle plots show that in spite the increase in the NH_3 to Mo ratio, the length of the α-MoO_3 nanorods remained unchanged. Moreover, the α-MoO_3 nanorods lengths are plotted as a function of the NH_3 to CA ratio. It seems to decrease as the NH_3 to CA ratio increases, as shown in the inset graph of Fig. 6d. However, samples with the same ratio of Mo to CA (open circle) are displayed, and the α-MoO_3 nanorods lengths remained unchanged even if the NH_3 to CA ratio increases. These results show that the intrinsic amount of NH_3 does not

affect the growth of α-MoO_3 nanorods.

As a consequence, this has demonstrated that increasing of the NH_3 amount in the precursor has the reducing effects on both the number of the v nanorods and plate-like α-MoO_3 crystals without the effective growth of the length of nanorods. Moreover, the plots of sample D(1:3:2) showed almost identical tendencies as sample C(1:3:2) in all of Fig. 6a – d. The results suggest that the NH_3 concentration in the precursor can be controlled regardless of the ammonium molybdate reagent.

CONCLUSIONS

The formation mechanism of the molybdenum oxide nanostructure, that is, nanorods and plate-like crystals on the seed layer by the MOD method, was examined in this study. The details of α-MoO_3 nanorods growth in molybdenum oxide thin films and the phase transition to plate-like α-MoO_3 crystals of α-MoO_3 nanorods were investigated, with the controlled precursors coating thickness under each spin-coating condition. The precursor viscosities were changed through the mixing ratios of the raw materials, such as molybdenum (Mo), citric acid (CA), ammonium (NH_3), and solvent.

The additive effect of CA in the precursor was investigated in detail with α-MoO_3 nanorods growth. The result implied that the length of the grown α-MoO_3 nanorods increased

with an increase in the CA to Mo ratio, which implies that CA is an essential agent for α-MoO_3 nanorods growth. In addition, the α-MoO_3 crystal growth was examined considering the influence of the coating film thickness by changing the spin-coating conditions. The result implies that the phase transition from the α-MoO_3 nanorods to the plate-like α-MoO_3 crystals is highly dependent on the thickness of the as-deposited film coating. In optimizing the as-deposited coating thickness, only the α-MoO_3 nanorods grew significantly; however, when the thickness of the coating was thin, the number of plate-like α-MoO_3 crystals increased because of the occurrence of the phase transition of α-MoO_3 nanorods. When the film thickness was extremely thin after coating, almost all the α-MoO_3 nanorods underwent the phase transition and formed large number of plate-like α-MoO_3 crystals.

The correlation between the seed layer thickness and the α-MoO_3 crystal after sintering was also investigated. The number of α-MoO_3 nanorods significantly increased with increasing seed layer thickness, but the number of plate-like α-MoO_3 crystals sharply decreased at approximately 50 nm of the seed layer thickness after sintering at 673 K for 15 min. The results suggest that the phase transition from α-MoO_3 nanorods to plate-like α-MoO_3 crystals proceeded rapidly when the seed layer thickness was less than 50 nm after sintering. Based on these results and the fact that the α-MoO_3 nanorods grew in the initial stage of the sintering, and then underwent the phase transition to the plate-like α-MoO_3 crystals in the second stage. This leads the study implies that the as-deposited thicknesses after spin coating are important

factors for the numbers of α-MoO_3 nanorods and plate-like α-MoO_3 crystals.

Furthermore, the effects of the growth of α-MoO_3 nanorods and the transition to the plate-like α-MoO_3 crystals were investigated with the amounts of CA and NH_3 to Mo in the precursor. The large amount of NH_3 to CA in the precursor suppressed the thermal decomposition of CA, and the α-MoO_3 nanorods could be extended without the phase transition to the plate-like α-MoO_3 crystals. The results of the experiments clarified that the CA role for α-MoO_3 nanorods growth and extension, and the existence of NH_3 make delayed the decomposition timing of CA; consequently, the phase transition to plate-like α-MoO_3 crystal timing could be controlled by changing the ratio of NH_3 to CA in the precursor.

From these results, it is concluded that the α-MoO_3 nanorods thin-film structure, that is, the α-MoO_3 nanorods length, the seed layer thickness, and the number of plate-like α-MoO_3 crystals, can be controlled by varying the amount of CA and NH_3 in the precursor and the thickness of the spin-coated film. Moreover, using the methods proposed in this study, we demonstrated the fabrication of transparent thin films with α-MoO_3 nanorods; the longest nanorod length was almost 1 micrometer. A detailed control technique to obtain an molybdenum oxide thin-film nanostructure was obtained in this research, which is a process to produce nanostructured thin films in a short time. This method may contribute to the development of various technologies for sustainable low energy societies in the future.

ACKNOWLEDGMENTS

A part of this work is supported by Grant-in-Aid for Challenging Exploratory Research Grant Numbers “16K13637” and the Programs for JST CREST Grant Number of “JP MJCR19J1” from Japan Science and Technology Agency(JST). In addition, all authors acknowledge funding of a part of this work from “Dynamic Alliance for Open Innovation Bridging Human, Environment and Materials” in “Network Joint Research Center for Materials and Devices” from the Ministry of Education, Culture, Sports, Science and Technology of Japan (MEXT).

REDERENCES

(1) Zhang, Z.; Yang, R.; Gao, Y.; Zhao, Y.; Wang, J.; Huang, L.; Guo, J.; Zhou, T.; Lu, P.; Guo, Z.; Wang, Q. Novel Na2Mo4O13/α-MoO3hybrid Material as Highly Efficient CWAO Catalyst for Dye Degradation at Ambient Conditions. *Sci. Rep.* **2014**, *4*, 1–9. https://doi.org/10.1038/srep06797.

(2) Liu, Y.; Feng, P.; Wang, Z.; Jiao, X.; Akhtar, F. Novel Fabrication and Enhanced Photocatalytic MB Degradation of Hierarchical Porous Monoliths of MoO3 Nanoplates. *Sci. Rep.* **2017**, *7* (1), 1–12. https://doi.org/10.1038/s41598-017-02025-3.

(3) Miao, J.; Xiao, F. X.; Bin Yang, H.; Khoo, S. Y.; Chen, J.; Fan, Z.; Hsu, Y. Y.; Ming Chen, H.; Zhang, H.; Liu, B. Hierarchical Ni-Mo-S Nanosheets on Carbon Fiber Cloth: A Flexible Electrode for Efficient Hydrogen Generation in Neutral Electrolyte. *Sci. Adv.* **2015**, *1* (7). https://doi.org/10.1126/sciadv.1500259.

(4) Zhang, L.; Zheng, S.; Wang, L.; Tang, H.; Xue, H.; Wang, G.; Pang, H. Fabrication of Metal Molybdate Micro/Nanomaterials for Electrochemical Energy Storage. *Small* **2017**, *13* (33), 1–19. https://doi.org/10.1002/smll.201700917.

(5) Choi, M.; Park, Y. J.; Sharma, B. K.; Bae, S. R.; Kim, S. Y.; Ahn, J. H. Flexible Active-Matrix Organic Light-Emitting Diode Display Enabled by MoS2 Thin-Film Transistor. *Sci. Adv.* **2018**, *4* (4), 1–8. https://doi.org/10.1126/sciadv.aas8721.

(6) Zhong, M.; Shen, C.; Huang, L.; Deng, H. X.; Shen, G.; Zheng, H.; Wei, Z.; Li, J. Electronic Structure and Exciton Shifts in Sb-Doped MoS2 Monolayer. *npj 2D Materials and Applications*. 2019. https://doi.org/10.1038/s41699-018-0083-1.

(7) Cong, S.; Sugahara, T.; Wei, T.; Jiu, J.; Hirose, Y.; Nagao, S.; Suganuma, K. Diverse Adsorption/Desorption Abilities Originating from the Nanostructural Morphology of VOC Gas Sensing Devices Based on Molybdenum Trioxide Nanorod Arrays. *Adv. Mater. Interfaces* **2016**, *3* (14), 1–8. https://doi.org/10.1002/admi.201600252.

(8) Xiao, S. J.; Zhao, X. J.; Chu, Z. J.; Xu, H.; Liu, G. Q.; Huang, C. Z.; Zhang, L. New Off-On Sensor for Captopril Sensing Based on Photoluminescent MoOx Quantum Dots. *ACS Omega* **2017**, *2* (4), 1666–1671. https://doi.org/10.1021/acsomega.7b00088.

(9) Archanjo, B. S.; Siles, P. F.; Oliveira, C. K. B. Q. M.; Baptista, D. L.; Neves, B. R. A. Characterization of Metal Oxide-Based Gas Nanosensors and Microsensors Fabricated via Local Anodic Oxidation Using Atomic Force Microscopy. *Adv. Mater. Sci. Eng.* **2013**, *2013*. https://doi.org/10.1155/2013/898565.

(10) Jiang, X. Y.; Zhang, Z. L.; Cao, J.; Khan, M. A.; Khizar-Ul-Haq; Zhu, W. Q. White OLED with High Stability and Low Driving Voltage Based on a Novel Buffer Layer MoOx. *J. Phys. D. Appl. Phys.* **2007**, *40* (18), 5553–5557. https://doi.org/10.1088/0022-3727/40/18/007.

(11) Greiner, M. T.; Lu, Z. H. Thin-Film Metal Oxides in Organic Semiconductor Devices: Their Electronic Structures, Work Functions and Interfaces. *NPG Asia Mater.* **2013**, *5*

(7), 1–16. https://doi.org/10.1038/am.2013.29.

(12) Cong, S.; Hadipour, A.; Sugahara, T.; Wei, T.; Jiu, J.; Ranjbar, S.; Hirose, Y.; Karakawa, M.; Nagao, S.; Aernouts, T.; Suganuma, K. Modifying the Valence State of Molybdenum in the Efficient Oxide Buffer Layer of Organic Solar Cells via a Mild Hydrogen Peroxide Treatment. *J. Mater. Chem. C* **2017**, *5* (4), 889–895. https://doi.org/10.1039/c6tc04461a.

(13) Hasani, A.; Van Le, Q.; Nguyen, T. P.; Choi, K. S.; Sohn, W.; Kim, J. K.; Jang, H. W.; Kim, S. Y. Facile Solution Synthesis of Tungsten Trioxide Doped with Nanocrystalline Molybdenum Trioxide for Electrochromic Devices. *Sci. Rep.* **2017**, *7* (1), 1–10. https://doi.org/10.1038/s41598-017-13341-z.

(14) Lei, Z.; Yang, X.; Dong, J.; Yi, X. Novel Metastable Hexagonal MoO3 Nanobelts: Synthesis, Photochromic, and Electrochromic Properties. *Chem. Mater.* **2009**, *21* (23), 5681–5690. https://doi.org/10.1021/cm9023887.

(15) El Moll, H.; Dolbecq, A.; Mbomekalle, I. M.; Marrot, J.; Deniard, P.; Dessapt, R.; Mialane, P. Tuning the Photochromic Properties of Molybdenum Bisphosphonate Polyoxometalates. *Inorg. Chem.* **2012**, *51* (4), 2291–2302. https://doi.org/10.1021/ic202299d.

(16) Li, X.; Yang, X.; Xue, H.; Pang, H.; Xu, Q. Metal–Organic Frameworks as a Platform for Clean Energy Applications. *EnergyChem* **2020**, *2* (2), 100027. https://doi.org/10.1016/j.enchem.2020.100027.

(17) Li, Q.; Li, N.; An, J.; Pang, H. Controllable Synthesis of a Mesoporous NiO/Ni Nanorod as an Excellent Catalyst for Urea Electro-Oxidation. *Inorg. Chem. Front.* **2020**, *7* (10), 2089–2096. https://doi.org/10.1039/d0qi00316f.

(18) de Castro, I. A.; Datta, R. S.; Ou, J. Z.; Castellanos-Gomez, A.; Sriram, S.; Daeneke, T.; Kalantar-zadeh, K. Molybdenum Oxides – From Fundamentals to Functionality. *Adv. Mater.* **2017**, *29* (40), 1–31. https://doi.org/10.1002/adma.201701619.

(19) Aji, A. S.; Nishi, R.; Ago, H.; Ohno, Y. High Output Voltage Generation of over 5 V from Liquid Motion on Single-Layer MoS2. *Nano Energy* **2020**, *68* (October 2019), 104370. https://doi.org/10.1016/j.nanoen.2019.104370.

(20) Lou, S. N.; Yap, N.; Scott, J.; Amal, R.; Ng, Y. H. Influence of MoO3 (110) Crystalline Plane on Its Self-Charging Photoelectrochemical Properties. *Sci. Rep.* **2014**, *4* (110). https://doi.org/10.1038/srep07428.

(21) Lou, X. W.; Zeng, H. C. Hydrothermal Synthesis of α-MoO3 Nanorods via Acidification of Ammonium Heptamolybdate Tetrahydrate. *Chem. Mater.* **2002**, *14* (11), 4781–4789. https://doi.org/10.1021/cm0206237.

(22) Kaindl, R.; Bayer, B. C.; Resel, R.; Müller, T.; Skakalova, V.; Habler, G.; Abart, R.; Cherevan, A. S.; Eder, D.; Blatter, M.; Fischer, F.; Meyer, J. C.; Polyushkin, D. K.; Waldhauser, W. Growth, Structure and Stability of Sputter-Deposited MoS2 Thin

Films. *Beilstein J. Nanotechnol.* **2017**, *8* (1), 1115–1126. https://doi.org/10.3762/bjnano.8.113.

(23) Liu, C.; Li, Z.; Zhang, Z. MoOx Thin Films Deposited by Magnetron Sputtering as an Anode for Aqueous Micro-Supercapacitors. *Sci. Technol. Adv. Mater.* **2013**, *14* (6). https://doi.org/10.1088/1468-6996/14/6/065005.

(24) Elamurugu, E.; Shanmugam, P.; Gonçalves, G.; Franco, N.; Alves, E.; Martins, R.; Fortunato, E. The Electronic Transport Mechanism in Indium Molybdenum Oxide Thin Films RF Sputtered at Room Temperature. *Epl* **2012**, *97* (3). https://doi.org/10.1209/0295-5075/97/36002.

(25) Cong, S.; Sugahara, T.; Wei, T.; Jiu, J.; Hirose, Y.; Nagao, S.; Suganuma, K. Growth and Extension of One-Step Sol-Gel Derived Molybdenum Trioxide Nanorods via Controlling Citric Acid Decomposition Rate. *Cryst. Growth Des.* **2015**, *15* (9), 4536–4542. https://doi.org/10.1021/acs.cgd.5b00790.

(26) Sugahara, T.; Alipour, L.; Hirose, Y.; Ekubaru, Y.; Nakamura, J.; Ono, H.; Harada, N.; Suganuma, K. Formation of Metal-Organic Decomposition Derived Nanocrystalline Structure Titanium Dioxide by Heat Sintering and Photosintering Methods for Advanced Coating Process, and Its Volatile Organic Compounds' Gas-Sensing Properties. *ACS Appl. Electron. Mater.* **2020**. https://doi.org/10.1021/acsaelm.0c00237.

(27) Karakawa, M.; Sugahara, T.; Hirose, Y.; Suganuma, K.; Aso, Y. Thin Film of Amorphous Zinc Hydroxide Semiconductor for Optical Devices with an Energy-Efficient Beneficial Coating by Metal Organic Decomposition Process. *Sci. Rep.* **2018**, *8* (1), 1–7. https://doi.org/10.1038/s41598-018-27953-6.

(28) Araki, T.; Sugahara, T.; Jiu, J.; Nagao, S.; Nogi, M.; Koga, H.; Uchida, H.; Shinozaki, K.; Suganuma, K. Cu Salt Ink Formulation for Printed Electronics Using Photonic Sintering. *Langmuir* **2013**, *29* (35), 11192–11197. https://doi.org/10.1021/la402026r.

(29) Sugahara, T.; Hirose, Y.; Cong, S.; Koga, H.; Jiu, J.; Nogi, M.; Nagao, S.; Suganuma, K. Sol-Gel-Derived High-Performance Stacked Transparent Conductive Oxide Thin Films. *J. Am. Ceram. Soc.* **2014**, *97* (10), 3238–3243. https://doi.org/10.1111/jace.13116.

Table of Contents (TOC)

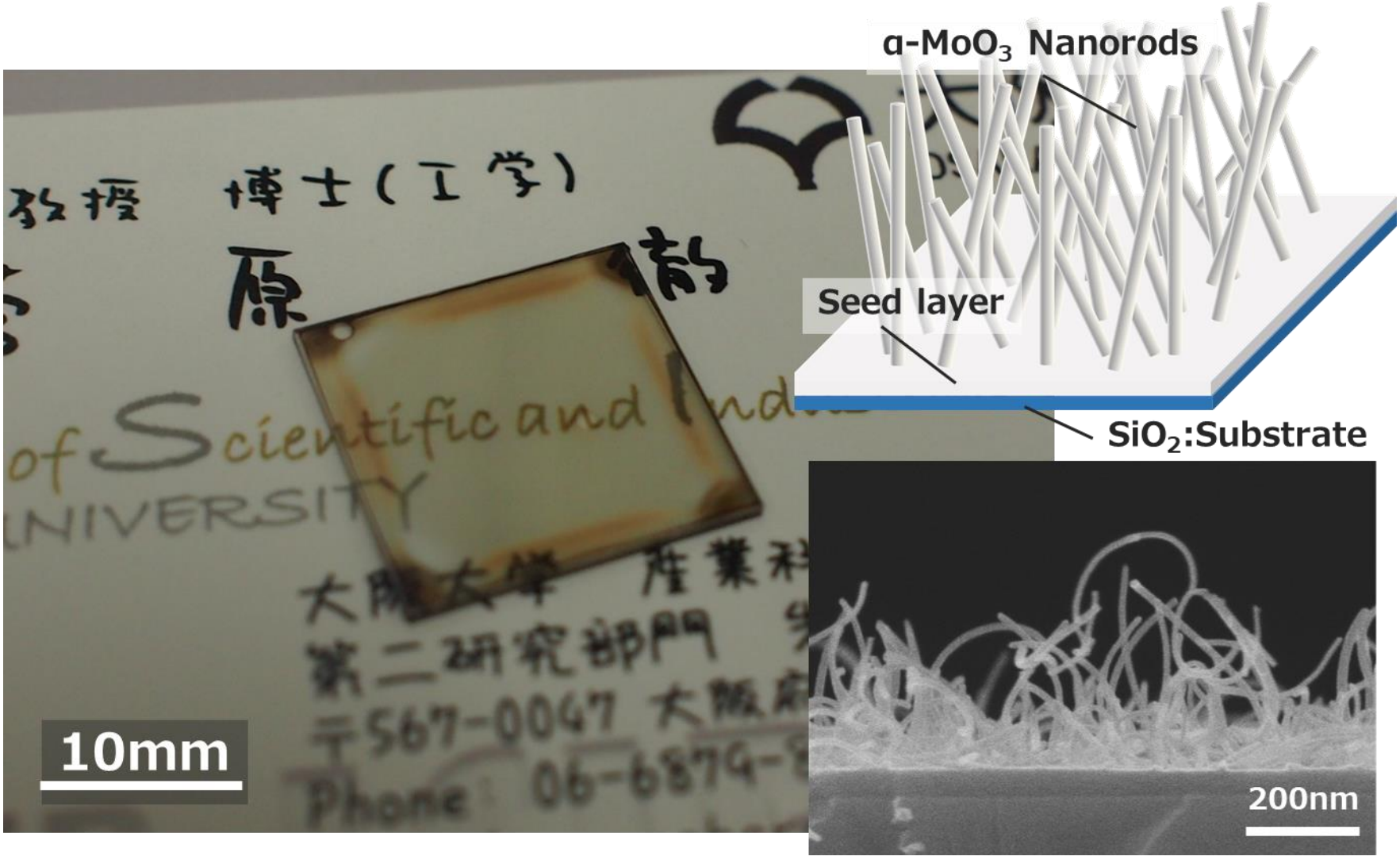

Table 1. The each experimental parameters of the precursors (Mo:0.5 M)

Sample Ratio / Mo : citric acid : NH_3	Viscosity [mPa. s] [*1]	Rotational speed of spin coating [rpm] [*2]	Thickness after drying 373K [μm]	Nanorods length [nm] [*3]	Seed layer thickness [nm] [*3]
1:3:2	9.6	1500	1.1	~400	~200
1:4:2	18.8	2000	1.0	~500	~100
1:6:2	89.2	3000	1.4	~1000	~50

[*1] The viscosity of the precursors measured at 298K and 1.1ml in the ambient atmosphere.

[*2] Spin coating conditions are fixed about 1 μm after drying at 373K for 15min.

[*3] The values of nanorods length and thickness are measured after sintering at 673K for 15min.

Table 2. The experimental parameters of the each precursors

Sample name	Molar Conc. / Mo	Weight Conc. of Mo [wt%]	Sample Ratio / Mo : citric acid: NH_3	Rotational speed of spin coating [rpm]	Thickness after drying [μm][*1]
A(1:6:2)	0.5M	7.5	1:6:2	3000	1.4
B(1:4:2)	0.5M	10.7	1:4:2	2000	1.0
C(1:3:2)	0.5M	13.6	1:3:2	1500	1.1
D(1:3:2)[*2]	0.5M	13.6	1:3:2	1500	1.3
E(1:3:1)	0.5M	13.9	1:3:1	1150	1.3
F(1:3:1)	1.0M	13.9	1:3:1	3000	1.8
G(1:1:1)	1.0M	31.5	1:1:1	1100	1.4

[*1]Spin coating conditions are fixed about 1 μm after drying at 373K for 15min.

[*2]The sample D(Mo: CA: NH_3 =1:3:2) is made form sample E(Mo: CA: NH_3 =1:3:1) + NH_3 to prepare the same condition of C(Mo: CA: NH_3 =1:3:2).

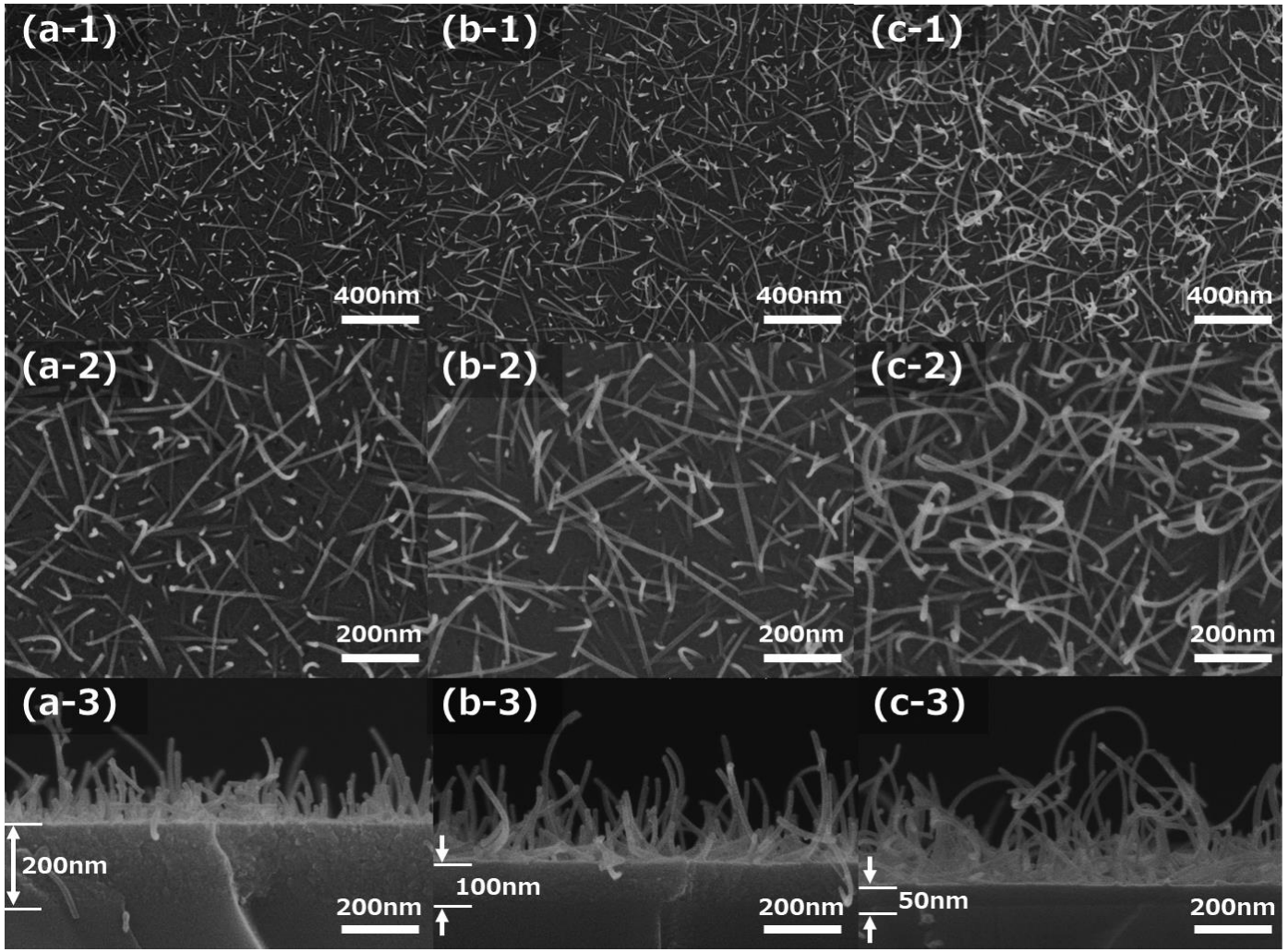

Figure 1. The top view / cross sectional FE-SEM Images of nanorods growth from seed layers fixed each experimental conditions after sintering at 673K for 15min. The film thickness are fixed as deposited by spin coating (a) 1500 rpm of the Mo: CA: NH_3 = 1:3:2, (b) 2000 rpm of the Mo: CA: NH_3 = 1:4:2, (c) 3000rpm of the Mo: CA: NH_3 = 1:6:2 samples, receptivity.

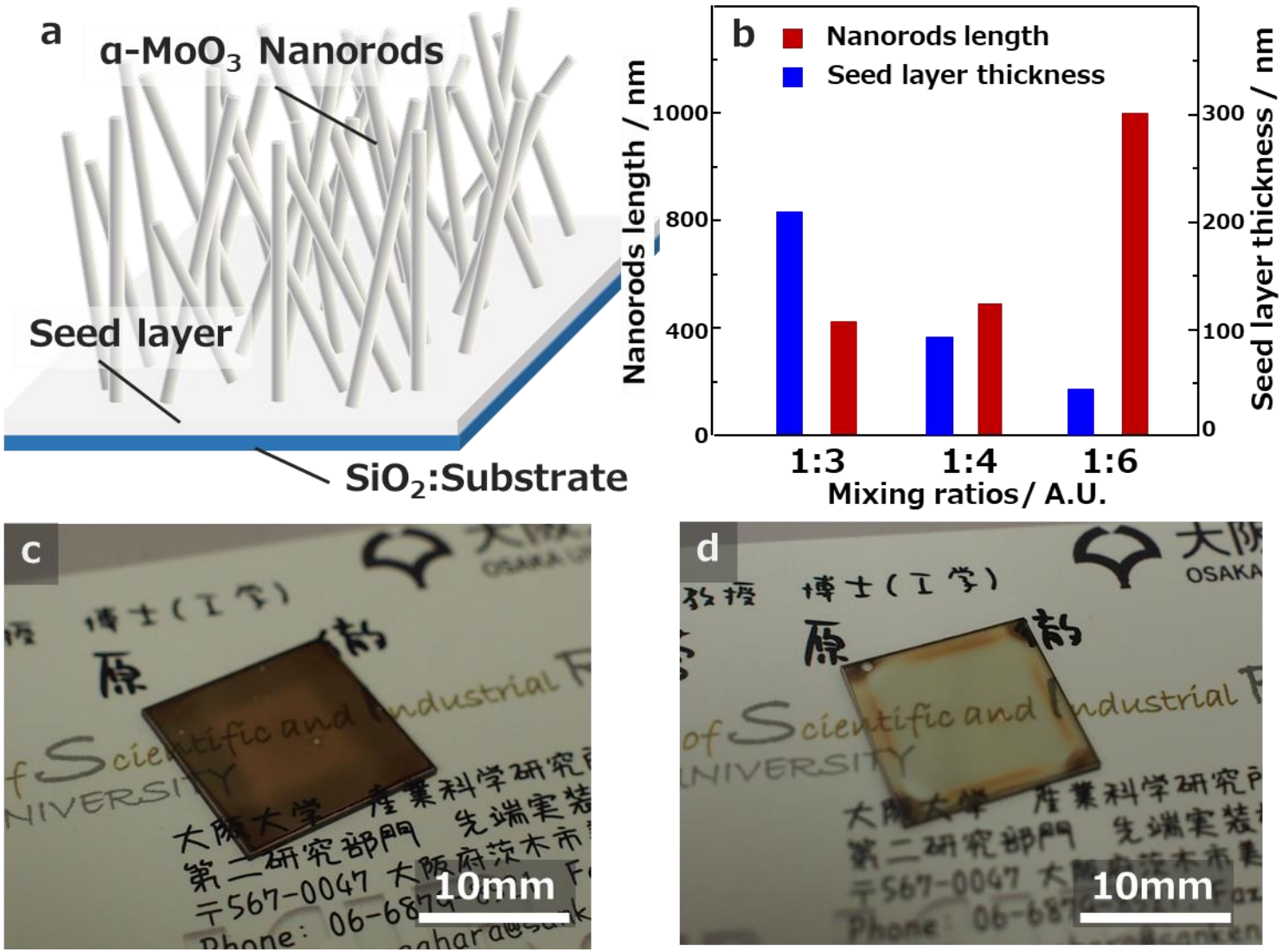

Figure 2. (a) The schematic figure of the α-MoO_3 nanorods film of α-MoO_3 nanorods growth from seed layer on the SiO_2 substrate. (b) The MoO_x nanorods length and the seed layer thicknesses of the each α-MoO_3 nanorods films. The photo figure images of each α-MoO_3 nanorods growth

from each seed layer thickness (c) about 200nm, and (d) about 50nm on the SiO_2 substrates.

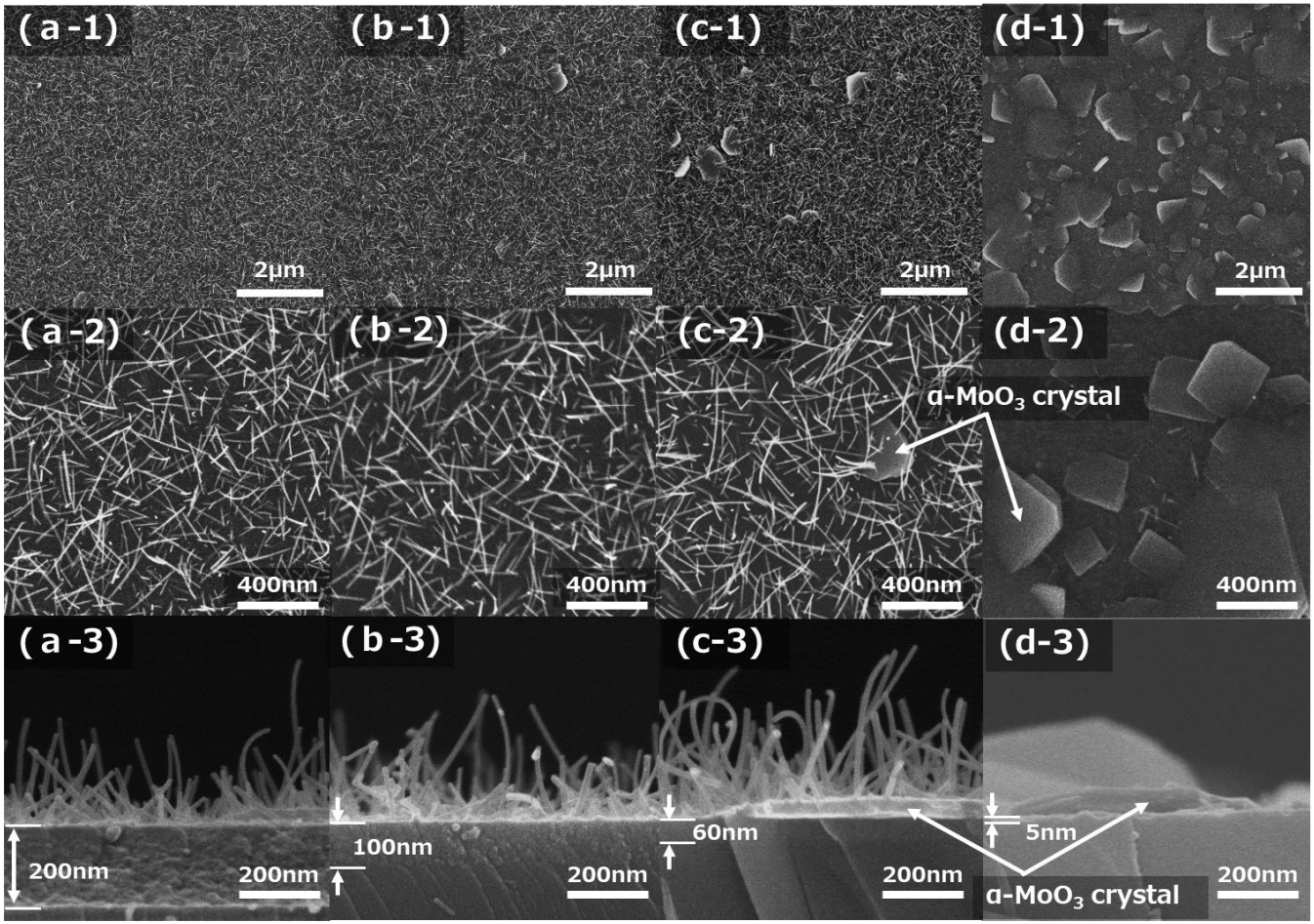

Figure 3. The top view / cross sectional FE-SEM Images of α-MoO_3 nanorods and crystals growth from seed layers after sintering at 673K for 15min. The as-deposited film thicknesses are controlled by spin coating condition each (a) 1500 rpm, (b) 2000 rpm, (c) 2500 rpm, (d) 5000rpm of the Mo: CA: NH_3 = 1:6:2 samples, receptivity.

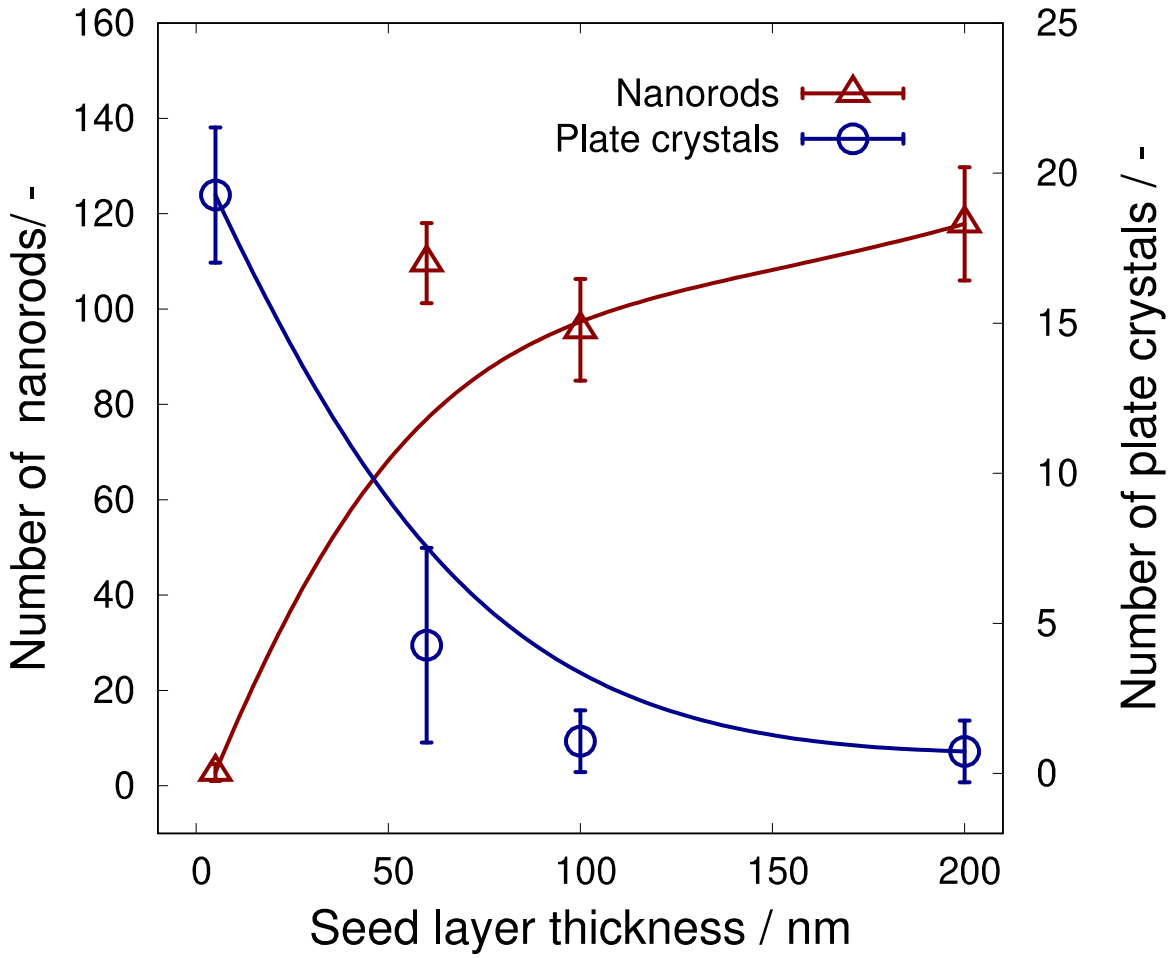

Figure 4. The α-MoO_3 nanorods numbers and α-MoO_3 plate-like crystals numbers as a function of the each seed layers thickness.

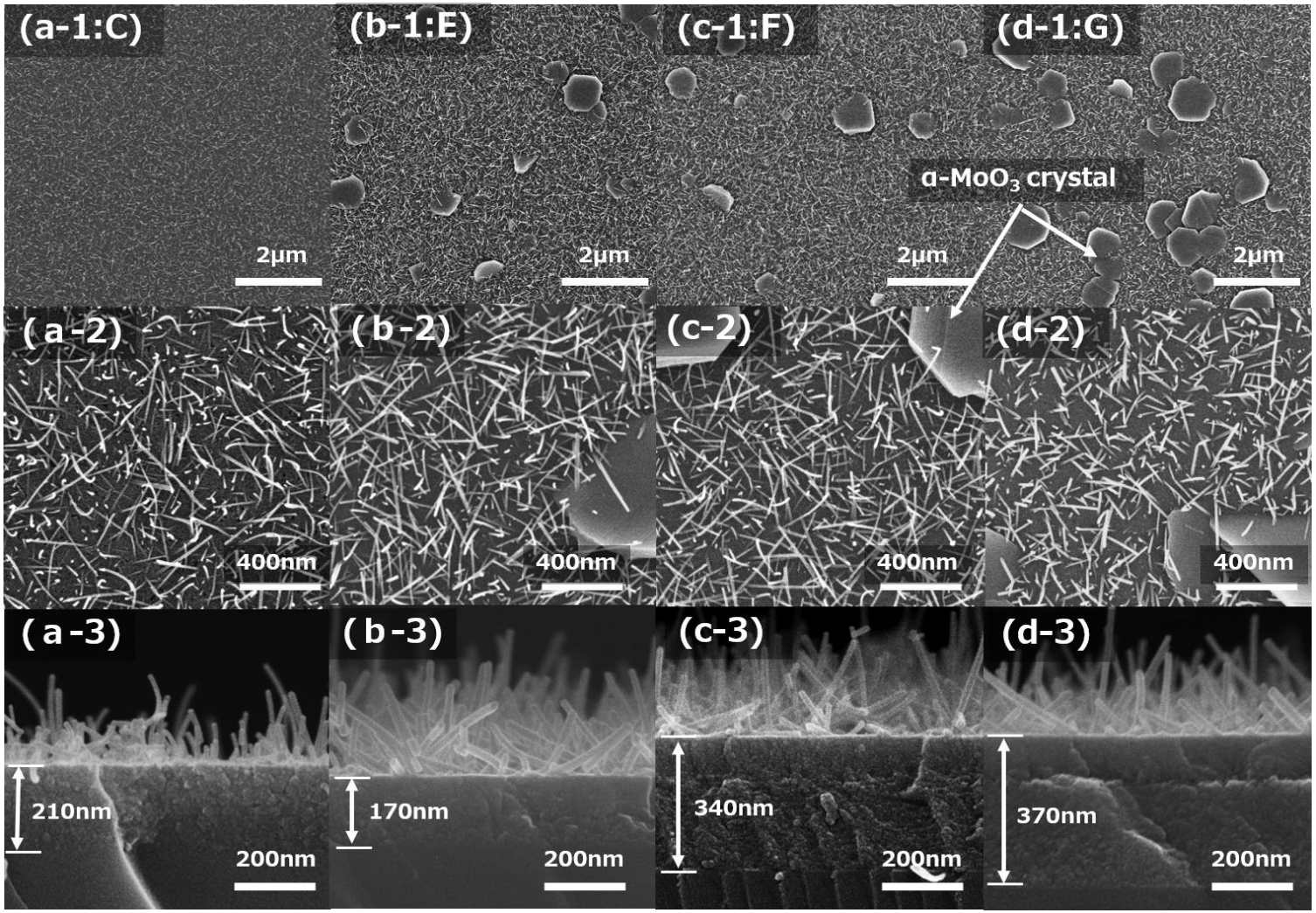

Figure 5. The top view / cross sectional FE-SEM Images of α-MoO_3 nanorods and crystals growth from seed layers after sintering at 673K for 15min. The film thickness are fixed at almost 1μm as deposited by spin coating of each (a) C(Mo: CA: NH_3 =1:3:2), (b) E(Mo: CA: NH_3 =1:3:1), (c) F(Mo: CA: NH_3 =1:3:1), and (d) G(Mo: CA: NH_3 =1:1:1) samples, receptivity.

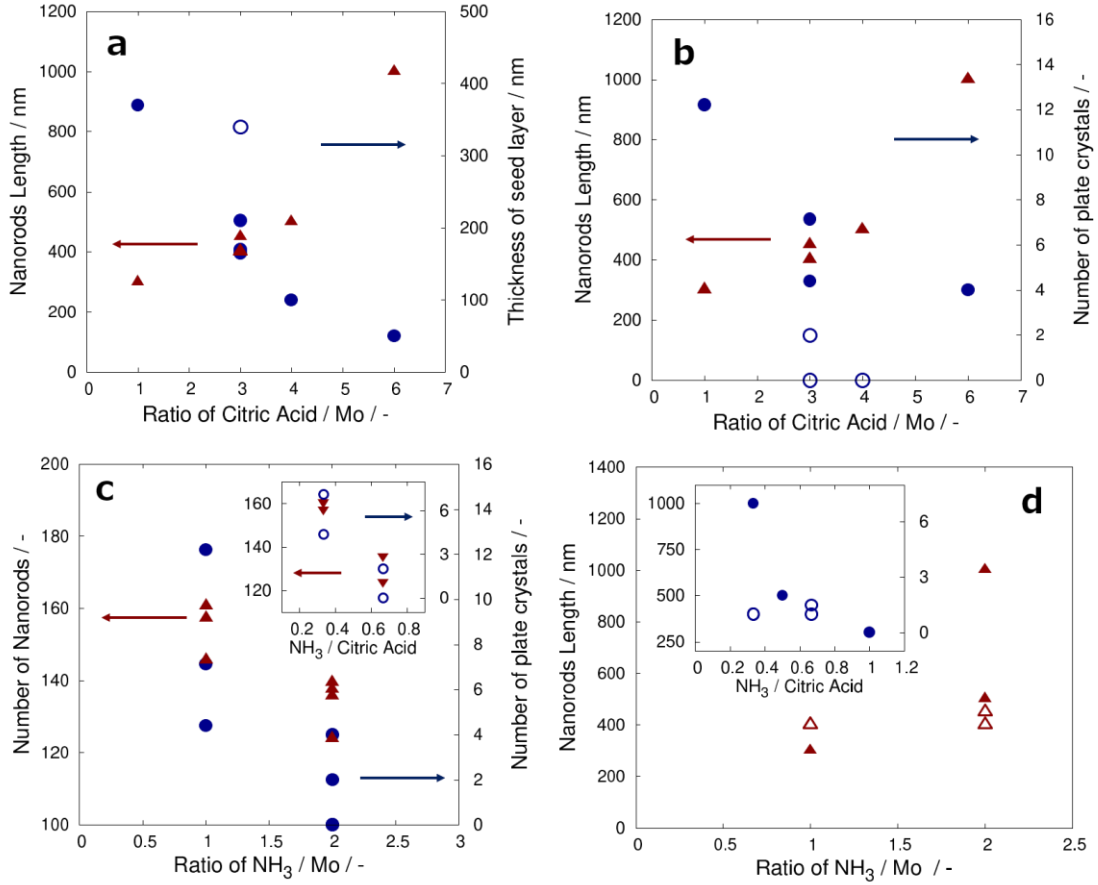

Figure 6. (a) The nanorods and the seed layer thickness versus citric acid / Mo ratios, and (b) The nanorods and the α-MoO_3 plate-like numbers versus citric acid / Mo ratios. (c) The nanorods and the α-MoO_3 plate-like numbers versus NH_3 / Mo ratios, and (d) The nanorods and the α-MoO_3 plate-like numbers versus NH_3 / Mo ratios. The each inset graphs are plotted as a function of NH_3 / citric acid ratios.